Online Signal Denoising Using Adaptive Stochastic Resonance in Parallel Array and Its Application to Acoustic Emission Signals

Jinki Kim[1]
Department of Mechanical Engineering,
Georgia Southern University,
P.O. Box 8046,
Statesboro, GA 30460
e-mails: jinkikim@georgiasouthern.edu;
jinkikim@umich.edu

Ryan L. Harne
Department of Mechanical Engineering,
The Pennsylvania State University,
336 Reber Building,
University Park, PA 16802-4400
e-mails: ryanharne@psu.edu;
rqh5445@psu.edu

K. W. Wang
Department of Mechanical Engineering,
University of Michigan,
2468 G.G. Brown Building,
2350 Hayward Street,
Ann Arbor, MI 48109-2125
e-mail: kwwang@umich.edu

Signal denoising has been significantly explored in various engineering disciplines. In particular, structural health monitoring applications generally aim to detect weak anomaly responses (including acoustic emission (AE)) generated by incipient damage, which are easily buried in noise. Among various approaches, stochastic resonance (SR) has been widely adopted for weak signal detection. While many advancements have been focused on identifying useful information from the frequency domain by optimizing parameters in a post-processing environment to activate SR, it often requires detailed information about the original signal a priori, which is hardly assessed from signals overwhelmed by noise. This research presents a novel online signal denoising strategy by utilizing SR in a parallel array of bistable systems. The original noisy input with additionally applied noise is adaptively scaled, so that the total noise level matches the optimal level that is analytically predicted from a generalized model to robustly enhance signal denoising performance for a wide range of input amplitudes that are often not known in advance. Thus, without sophisticated post-processing procedures, the scaling factor is straightforwardly determined by the analytically estimated optimal noise level and the ambient noise level, which is one of the few quantities that can be reliably assessed from noisy signals in practice. Along with numerical investigations that demonstrate the operational principle and the effectiveness of the proposed strategy, experimental validation of denoising AE signals by employing a bistable Duffing circuit system exemplifies the promising potential of implementing the new approach for enhancing online signal denoising in practice.
[DOI: 10.1115/1.4052639]

Keywords: stochastic resonance, signal processing, denoising, weak signal detection, acoustic emission, Duffing, bistable system, machinery noise, nonlinear vibration, random vibration

1 Introduction

Noise is unavoidable in measurements. For example, in structural health monitoring (SHM), the accuracy in assessing the structural integrity may be significantly undermined due to noise contamination in the measurement of damage-induced signals. Since structural damage often worsens over time to adversely affect the functioning of the system, it is imperative to identify incipient, small-sized damages. Yet, weak anomaly signals generated by incipient damage can easily be buried in noise. Therefore, accurately recovering the damage-induced signals from noise-contaminated measurements is one of the major challenges in SHM [1,2].

Among various methods, a nonlinear phenomenon called stochastic resonance (SR) has recently received significant attention for signal processing. Unlike other conventional methods that may weaken the original signal by generally filtering out the noise [3,4], SR may amplify the weak signal buried in noise by utilizing the attendant noise that is a free source of energy. Since the concept of SR was first introduced to assess the periodic recurrence of the Earth's ice ages [5,6], it has been observed from various phenomena in physical [7,8], chemical [9,10], biological [11–13], and social [14,15] systems. SR often refers to a phenomenon where a suitable amount of noise enhances the output signal quality, often the signal-to-noise ratio (SNR) in a nonlinear system [16,17]. For example, when right amount of noise is included in a weak input signal, a nonlinear system may exhibit a large periodic response that is statistically synchronized with the periodicity of the input signal. As a result, the output power spectral density corresponding to the periodic excitation frequency may be greatly increased and exhibit a peak when SR occurs. Due to this constructive role of noise when SR is activated, SR has been explored in a variety of contexts, such as biomedical systems [18,19], image processing [20,21], and fault diagnosis in mechanical systems [22–30].

The optimal amount of noise that activates SR has often been estimated based on a classical theoretical framework of time-scale matching that assumes adiabatic condition where the frequency and amplitude of the deterministic input signal and noise intensity are much smaller than unity [16,17]. Since the input signal in practical applications seldom satisfies the adiabatic assumption, SR has generally been employed by tuning the system parameters that adjust the restoring potential of the nonlinear system and/or by scaling the frequency of the input signal to utilize the classical theoretical framework of time-scale matching [23–33]. On the other hand, the system parameters, amplitude and frequency scaling

[1]Corresponding author.

Contributed by the Noise Control and Acoustics Division of ASME for publication in the Journal of Vibration and Acoustics. Manuscript received April 9, 2021; final manuscript received September 21, 2021; published online October 20, 2021. Assoc. Editor: Melih Eriten.

factors, are often determined by computationally expensive optimization algorithms in a post-processing environment based on the classical SR theory. Moreover, detailed information about the original signal are often required to be known a priori for optimized system parameter selections, which is hardly satisfied in practice especially when the signal is overwhelmed by noise. In addition, while SR has been exploited to successfully enhance SNR for weak signal detection in the frequency domain, for example, by identifying damage-induced frequency changes that become more prominent by SR, relatively little attention has been made to recover the time domain waveforms by harnessing SR.

To address these concerns, this research investigates a novel signal conditioning methodology for online signal denoising. This study focuses on exploring a new strategy that effectively utilizes the SR in an array of bistable systems to reduce noise and recover the original signal waveform by adaptively adjusting the input amplitude based on the analytically determined optimal noise level and the noise level of the given signal, which is one of the few quantities that may be identified from practical measurements overwhelmed by noise. The proposed approach is not limited to small-amplitude periodic input signals by exploiting the suprathreshold SR in bistable system array [18,34,35]. In the following sections, we first discuss the potential of utilizing SR for signal denoising in a parallel array of generalized bistable systems with additional noise applied to the input signal. Then, the analytical investigation that estimates optimal noise level and gain selection strategy for readily activating SR are introduced considering practical implementations for online signal denoising. Numerical investigations on denoising and recovering example acoustic emission (AE) signals and aperiodic signals verify the denoising performance of the new approach. Following proof-of-concept experimental investigations on AE signal denoising, concluding remarks are presented to summarize and reflect upon the potential of the new approach.

2 Stochastic Resonance in an Array of Bistable Systems for Signal Denoising

2.1 System Model Formulation. A parallel array of N identical bistable systems is considered for utilizing SR for signal denoising, as illustrated in Fig. 1. The original signal of interest $s(\tau)$ that is contaminated by zero-mean Gaussian white noise $\xi(\tau)$ with autocorrelation $\boldsymbol{\xi}(\boldsymbol{\tau})\boldsymbol{\xi}(0) = 2D_\xi\delta(\tau)$ is applied to the parallel array of bistable systems. Additional Gaussian white noise $\eta_j(\tau)$ with zero-mean is applied to the jth bistable system in the array, where $j = 1, 2, \ldots, N$. The additional noise $\eta_j(\tau)$ having a common noise intensity D_η are independent to each other and the original attendant noise $\xi(t)$. These signals are applied as input to each bistable system $\mathbf{S}_B$ following amplitude gain adjustments. The output signals $z_j(\tau)$ of each bistable system are averaged as $\bar{z}(\tau)$ to recover the original signal as shown in Fig. 1. A heavily damped bistable Duffing oscillator is employed as an archetypal model for the bistable systems in the array. Considering a heavily damped motion of a particle in a symmetric double-well potential, the inertia of the particle is ignored to obtain the non-dimensional governing equation as [16]

$$z_j'(\tau) = -\partial U(\tau)/\partial z + s(\tau) + \xi(\tau) + \eta_j(\tau) \tag{1}$$

The restoring potential of the oscillator is expressed as $U(z_j) = -z_j^2/2 + z_j^4/4$. $(\,)'$ indicates differentiation with respect to non-dimensional time τ. In this section, the original ambient noise $\xi(\tau)$ and gain adjustment are not considered ($D_\xi = 0$ and gain $G = 1$) to highlight the operational principle of utilizing SR for signal denoising.

Figure 2 demonstrates a numerical example of signal denoising using the algorithm presented in Fig. 1. In this example, we employ an amplitude modulated sine wave as an exemplary original signal of interest $s(\tau)$, which simulates a typical AE signal [2]:

$$s(\tau) = \frac{A}{2}\left[1 - \cos\left(\frac{2\pi f_o(\tau - \tau_d)}{N_{\text{cyc}}}\right)\right]\cos(2\pi f_o(\tau - \tau_d))\Pi(\tau) \tag{2}$$

Acoustic emission signals are transient high-frequency stress waves that are often utilized to identify incipient small-sized cracks in aerospace, mechanical, and civil structures. Since AE signals by small-sized damages may easily be buried in noise in practice, denoising is critical for AE-based SHM [2,36]. Further details on the AE signals with experimental investigation results are discussed in Sec. 4. $A = 0.3$ and $f_o = 0.006$, respectively, represent the maximum amplitude and frequency of the signal. $\tau_d = 539$ indicates the time when the amplitude modulated signal starts for $N_{\text{cyc}} = 10$ cycles. Here, $\Pi(\tau) = H(\tau - \tau_d) - H(\tau - (\tau_d + N_{\text{cyc}}/f_0))$ and $H(\tau)$ is the Heaviside step function.

Stochastic resonance is a phenomenon based on noise-activated saddle-node bifurcations. It is well known that a bistable Duffing oscillator may exhibit non-unique complex steady-state dynamics when the excitation frequency becomes close to the oscillator's linear natural frequency [34,37–39]. On the other hand, if the excitation frequency is much lower than the linear natural frequency, the excitation threshold that triggers saddle-node bifurcation becomes less influenced by the exact waveform of excitation $s(\tau)$ and its frequency since it approaches to the quasi-static bifurcation threshold. In this research, the bistable system is designed to exhibit a linear natural frequency that is much higher than the input signal frequency range in order to reliably activate the saddle-node

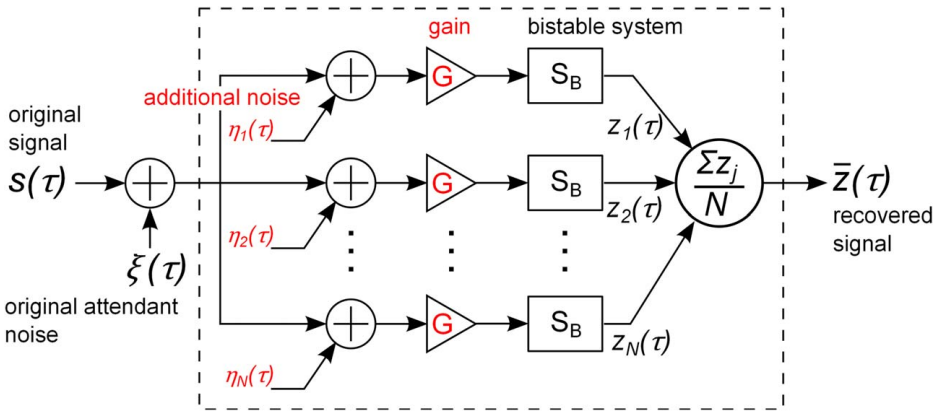

Fig. 1 Block diagram of the signal denoising algorithm using SR in an array of bistable systems

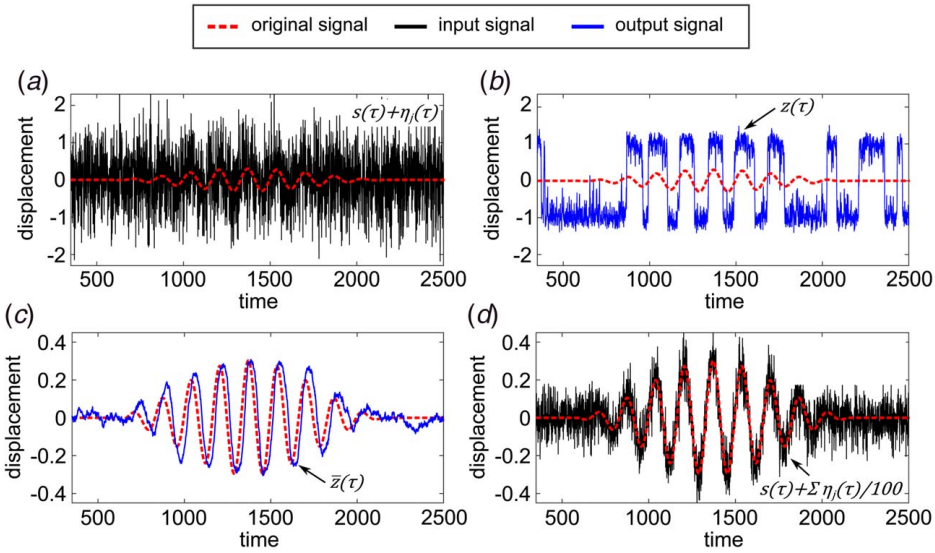

Fig. 2 (*a*) Input signal to the bistable array: a combination of the original signal $s\tau$ and additional noise $\eta_j(\tau)$, (*b*) example response of a single bistable system, (c) average of 100 output signals utilizing SR, and (*d*) average of 100 input signals (scaled with respect to the original signal amplitude for visual comparison). The original signal is shown (in dashed curve) in all plots as a reference.

bifurcation. As a result, the SR in the bistable system may be robustly realized regardless of the exact excitation form.

Figure 2(*a*) shows the signal $s(\tau)$ with additive Gaussian white noise $\eta_j(\tau)$, which is applied as input to 100 bistable systems. The noise independent to each other with a common intensity of $D_\eta = 0.26$ are generated using the MATLAB command randn. The responses of the bistable oscillators are obtained by numerically integrating Eq. (1) utilizing a fourth-order stochastic Runge–Kutta numerical method in MATLAB [40]. Figure 2(*b*) shows a representative response of the bistable oscillator. When the amplitude of the original signal $s(\tau)$ is zero ($\tau < 539$ or $\tau > 2206$), noise-activated large amplitude interwell transitions between the two stable equilibria of the bistable Duffing oscillator do not occur periodically in time. However, we can observe a trend of repeated interwell oscillations especially where the original signal $s(\tau)$ exists in the input signal, $539 \le \tau \le 2206$. Figure 2(*c*) presents the average $\bar{z}(\tau)$ of 100 output signals, which recovers the original sinusoidal signal with great quantitative agreement. The incoherent random transitions induced by the noise in each bistable element are averaged out to negligible amplitudes when the original signal is not included in the input. However, the original signal in combination with additional noise $\eta_j(\tau)$ activates statistically coherent interwell oscillations that become more prominent through the averaging process. As a result, the original signal is stochastically amplified in amplitude and approximately reconstructed. On the other hand, serving as a control for the proposed approach, Fig. 2(*d*) shows the output waveform obtained by simply averaging 100 runs of original signals with independently added noises without employing the array of bistable elements, which results in $s(\tau) + \sum_{j=1}^{100} \eta_j(\tau)/100$. It is observed that the averaged output signal of the bistable system array utilizing SR ($\bar{z}(\tau) = \sum_{j=1}^{100} z_j(\tau)/100$), shown in Fig. 2(*c*), exhibits remarkably superior denoising performance compared to the results shown in Fig. 2(*d*). In addition, the signal denoising results utilizing conventional filtering is provided in Appendix A. These results clearly demonstrate the merit and potential of utilizing the parallel array of bistable systems for SR-based signal denoising.

The SR in this study is based on considering a heavily damped motion of a particle driven by a zero-mean signal in a symmetric double-well potential. As a result, if the original signal has a non-zero bias, the output of each bistable element may tend to exhibit intrawell responses more frequent in the biased direction, which may result into a distorted waveform recovery. On the other hand, by asymmetrically designing the double-well potential to compensate the bias in the original signal, the proposed algorithm may be effectively applied for denoising input signals with non-zero-mean. For example, an asymmetric double-well potential $U_a(z_j) = a_0 z_j - z_j^2/2 + z_j^4/4$ compensates the non-zero bias a_0 in the original signal to yield an identical governing equation as Eq. (1):

$$\dot{z}_j(\tau) = -\partial U_a(\tau)/\partial z + s_a(\tau) + \xi(\tau) + \eta_j(\tau) \tag{3a}$$

$$= -\partial U(\tau)/\partial z + s(\tau) + \xi(\tau) + \eta_j(\tau) \tag{3b}$$

where $s_a(\tau) = a_0 + s(\tau)$ is the biased original signal.

2.2 Theoretical Framework for Stochastic Resonance in Parallel Array. We employ the sample Pearson's correlation coefficient (CC) [41] as a metric for characterizing SR and evaluating the signal denoising performance by quantifying the similarity between the original signal $s(\tau)$ and the denoised signal $\bar{z}(\tau)$; namely, CC closer to one implies superior signal denoising. Assuming $s(\tau)$ is a zero-mean signal, CC is defined as [34]

$$\mathrm{CC} = \max\left\{ \frac{(s(\tau) - s(\tau))(\bar{z}(\tau+\tau_d) - \bar{z}(\tau+\tau_d))}{\sigma_s \sigma_{\bar{z}}} \right\}$$
$$= \max\left\{ \frac{s(\tau)(\bar{z}(\tau+\tau_d) - \bar{z}(\tau+\tau_d))}{\sigma_s \sigma_{\bar{z}}} \right\} \tag{4}$$

where the angular brackets (…) denote an average over time, τ_d is a time lag, and $\sigma_X = \sqrt{(X(\tau) - X(\tau))^2}$ corresponds to the sample standard deviation of signal X. The phase shift between the output and the original signal is a well-known phenomenon associated with SR [16,42], which has been compensated when calculating the CCs. By assuming the random output $z_j(\tau)$ of each bistable system as a summation of its nonstationary ensemble average $E[z_j(\tau)]$ related to the deterministic original signal and a random fluctuation $\mu_j(\tau)$ induced by the total input noise $\xi(\tau) + \eta_j(\tau)$ around its mean [34,43,44], the recovered signal obtained by

ensemble averaging the outputs of N bistable systems is expressed as

$$\bar{z}(\tau) = E[z_j(\tau)] + \frac{1}{N}\sum_{j=1}^{N}\mu_j(\tau) \tag{5}$$

where $E[z_j(\tau)] = \int_{-z_\infty}^{z_\infty} \rho(z,\tau) z\, dz$. The probability density function $\rho(z, \tau)$ is obtained by numerically solving the Fokker–Planck equation associated with Eq. (1) for $z_\infty \gg 1$. Assuming the random fluctuation $\mu_j(\tau)$ in the output is independent of $E[z_j(\tau)]$ and monotonically increases with the total random input $\xi(\tau)+\eta_j(\tau)$, we estimate $\mu_j(\tau)=0$ and $\mu_j^2(\tau) = K_\mu D$ is proportional to that of the total input noise intensity $D = D_\xi + D_\eta$, where K_μ is a constant. Thus, the sample variance of the recovered signal can be expanded as follows:

$$\begin{aligned}\sigma_{\bar{z}}^2 &= \mathrm{var}\left(E[z_j(\tau)] + \frac{1}{N}\sum_{j=1}^{N}\mu_j(\tau)\right)\\ &= \mathrm{var}(E[z_j(\tau)]) + \mathrm{var}\left(\frac{1}{N}\sum_{j=1}^{N}\mu_j(\tau)\right)\end{aligned} \tag{6}$$

As a result, the standard deviation of the recovered signal is determined as

$$\sigma_{\bar{z}} = \left[E[z_j(\tau)]^2 - E[z_j(\tau)]^2 + \frac{1}{N}\mu_j^2(\tau)\right]^{1/2} \tag{7}$$

Substituting Eqs. (5) and (7) into Eq. (4) yields an expression for the signal denoising performance (CC) of the parallel array with N elements as

$$\mathrm{CC} = \max\left\{\frac{s(\tau)E[z_j(\tau+\tau_d)] + (1/N)\sum s(\tau)\mu_j(\tau+\tau_d)}{\sigma_s[E[z_j(\tau+\tau_d)]^2 - E[z_j(\tau+\tau_d)]^2 + ((\mu_j^2(\tau+\tau_d))/N)]^{1/2}}\right\} \tag{8}$$

The analytical predictions of the signal denoising performance (CC) from Eq. (8) for an N-element bistable system array are plotted as solid curves against $\sqrt{2D}$ in Fig. 3. Alongside the analytical results, numerical values are presented as markers, which are obtained by extending the numerical case study in Sec. 2.1 for various numbers of bistable elements in the array and additional noise levels while keeping other conditions the same. Figure 3 clearly displays a non-monotonic trend of CC values with respect to the total noise level, which is the characteristic behavior of SR [16,45]. It can be observed from Fig. 3 that the theoretical curves

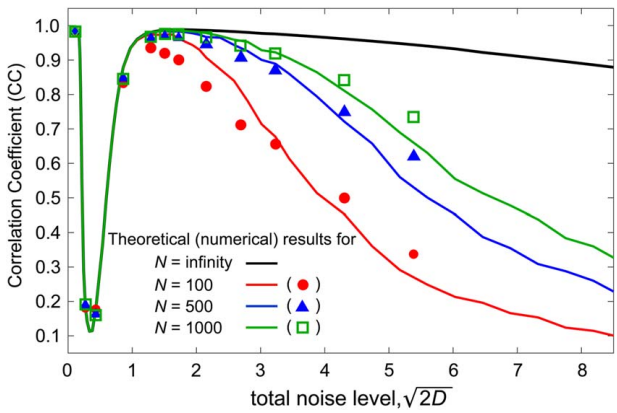

Fig. 3 Signal denoising performance (CC) as a function of noise level. The analytical predictions with $K\mu = 0.188$ (solid curves) from Eq. (8) are in good quantitative agreement with the numerically obtained values (symbols).

are in good agreement with the numerical results, predicting that as the number (N) of bistable elements in the parallel array increases, CC asymptotically approaches to a plateau near CC = 1 for a wide range of noise levels. It is worth noting that the CC derived in Eq. (8) is a general form without reference to any particular form of bistable system in the parallel array or the original signal waveforms. Thus, the analytical estimation of the CC and the optimal noise level that provides maximum signal denoising performance may be utilized for various systems that exploit SR in array of bistable elements.

2.3 Optimal Noise Level for Signal Denoising. The investigations presented in Sec. 2.2 demonstrate the potential of utilizing SR by introducing an optimal quantity of noise for signal denoising. While SR occurs by the interplay among the potential barrier of the bistable system, the input signal, and noise, we focus on tailoring the optimal noise level rather than modifying the original signal or the bistable system parameters that may be difficult to practically implement. The optimal noise level observed in Fig. 2 is found for an original input signal with certain amplitude ($A = 0.3$ in Eq. (2)). On the other hand, the optimal noise level that maximizes the SR effect for denoising may depend on the amplitude of the original signal. Figure 4(*a*) presents analytically predicted signal denoising performance as a function of the noise level $\sqrt{2D}$ and the amplitude of original signal $s(\tau)$. From Fig. 4(*a*), it is observed that the optimal noise level (indicated as circles) that maximizes the signal denoising performance (CC) is dependent on the amplitude of the original signal. Thus, the results in Fig. 4(*a*) clearly show that the information about the original signal amplitude is essential for determining the optimal noise level for signal denoising. However, in practice where the original signal may severely be corrupted by noise, it may be extremely challenging to accurately assess the original signal amplitude in advance to determine the corresponding optimal additive noise level. On the other hand, a favorable operational condition can be observed in Fig. 4(*a*) denoted by a dashed line box, where great signal denoising performance is obtained for a wide range of original input amplitudes. It is worth noting that we can identify an optimal noise intensity $D_{\mathrm{opt}} = 0.72$ that maximizes the average signal denoising performance over a broad range of original signal amplitudes encompassing both subthreshold and suprathreshold input signals from Fig. 4(*b*). Note that the original input signal is subthreshold if its amplitude is smaller than the static bifurcation threshold $A_c = 2/\sqrt{27} \approx 0.385$, and suprathreshold otherwise [35,44]. Thus, in the proposed approach, the input amplitude is not limited to be relatively small compared to the bistable potential threshold. While D_{opt} is not the optimal noise level for each input amplitude, it provides desirable signal denoising performance for a wide range of input amplitudes considering that the true amplitude of the original signal of interest is hardly assessed from noisy signals and generally not known a priori in practice. Therefore, we focus on utilizing this noise level D_{opt} as a practical key value for operating the proposed denoising strategy.

3 Operational Principle Detail and Numerical Demonstration

3.1 Overview of Denoising Procedure for Practical Implementation. The investigations in Sec. 2 are conducted without considering the original attendant noise $\xi(\tau)$ and gain adjustment shown in Fig. 1 to demonstrate the potential of utilizing SR for signal denoising. This section describes the SR-based denoising procedure considering the practical issues for implementation including the original ambient noise and gain adjustments to realize the optimal noise level discussed in Sec. 2.3. As illustrated in Sec. 2, the core principle of utilizing the SR in the array of bistable systems for signal denoising is to average out the noise-induced incoherent interwell transitions while enhancing the stochastically

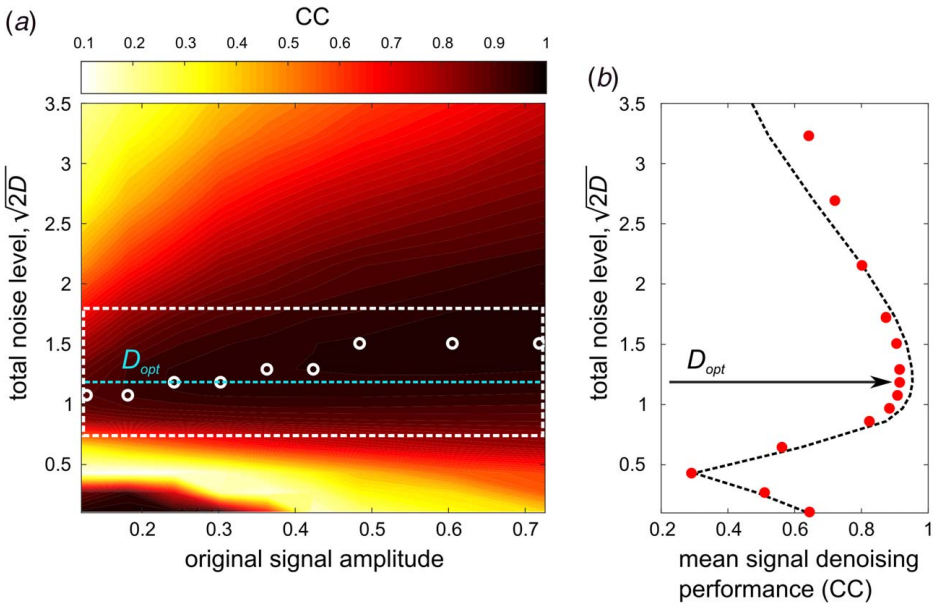

Fig. 4 (*a*) Analytically estimated signal denoising performance (CC) as a function of the original signal amplitude and total noise level. The optimal noise levels for each amplitude of the original signal are indicated as circles. The dashed line box indicates a key operational area that exhibits great signal denoising performance for a broad range of original signal amplitudes. (*b*) Analytical (dashed curve) and numerical (filled circles) results of the mean signal denoising performances over original signal amplitudes are presented with respect to the total noise level. D_{opt} in both figures indicates the optimal noise level that maximizes the average signal denoising performance over a broad range of original signal amplitudes.

coherent interwell transitions that are activated by the original signal. As a result, it is essential that the total noise ($\xi(\tau)+\eta_j(\tau)$ of Fig. 1) applied to each bistable system should be uncorrelated to each other. In other words, the additional noise $\eta_j(\tau)$ should be large enough to *contaminate* the original attendant noise $\xi(\tau)$ that is commonly applied to all bistable elements in the array. For example, if the additional noise is negligible compared to the original attendant noise, the input signals $s(\tau)+\xi(\tau)+\eta_j(\tau)$ to each bistable element may be correlated to each other, resulting in correlated responses that may provide little improvement in recovering the original signal by averaging. If the additional noise intensity is assumed as $D_\eta = r^2 D_\xi$, the CC between the total noises for each bistable circuit can be determined as

$$\widetilde{\mathrm{CC}}(\xi+\eta_j,\ \xi+\eta_k) = \frac{\mathrm{cov}(\xi+\eta_j,\ \xi+\eta_k)}{\sigma_{\xi+\eta_j}\sigma_{\xi+\eta_k}} \tag{9a}$$

$$= \frac{1}{r^2+1},\ j \neq k \tag{9b}$$

Assuming the signals have negligible correlation when $\widetilde{\mathrm{CC}}$ is less than 0.1, in this study, we apply additional noise that has nine times larger intensity ($r=3$) than that of the input noise, which yields $\widetilde{\mathrm{CC}}=0.1$ and the total noise intensity $D = 10\,D_\xi$. Then, the noisy input signal $s(\tau)+\xi(\tau)$ with additional noise $\eta_j(\tau)$ becomes the input for each bistable element following gain adjustment. In order to exploit the key operational condition discussed in Sec. 2.3, which provides great signal denoising performance for a broad range of original signal amplitudes, amplitude gain G is applied so that the total noise intensity of the adjusted input G^2D matches the optimal noise intensity D_{opt}. As a result, the gain G can be obtained as

$$G = \sqrt{\frac{D_{\mathrm{opt}}}{10\,D_\xi}} \tag{10}$$

The output signals of the bistable elements are then averaged to recover the original signal. If the ambient noise level changes (D'_ξ), the additional noise level ($D'_\eta = 10\,D'_\xi$) and gain values in Eq. (10) are adaptively updated to utilize the optimal noise level D_{opt} as illustrated in Fig. 5.

It should be noted that (1) we take advantage of the analytically estimated optimal quantity of noise D_{opt} to recover the original signal by effectively activating SR in the array of bistable systems, which does not require operating sophisticated optimization algorithms in a post-processing environment for selecting scaling parameters, thus enabling online signal denoising; (2) the optimal noise intensity D_{opt} is determined based on a generalized bistable Duffing oscillator in Eq. (1) without any reference to

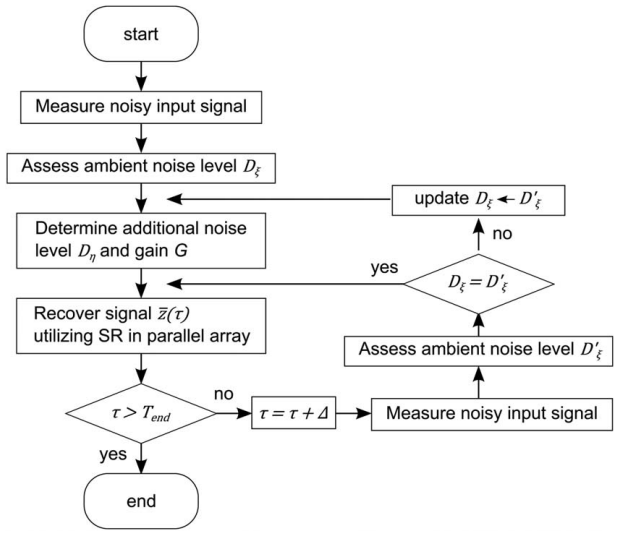

Fig. 5 Flowchart of the proposed signal denoising approach utilizing adaptive SR in parallel array

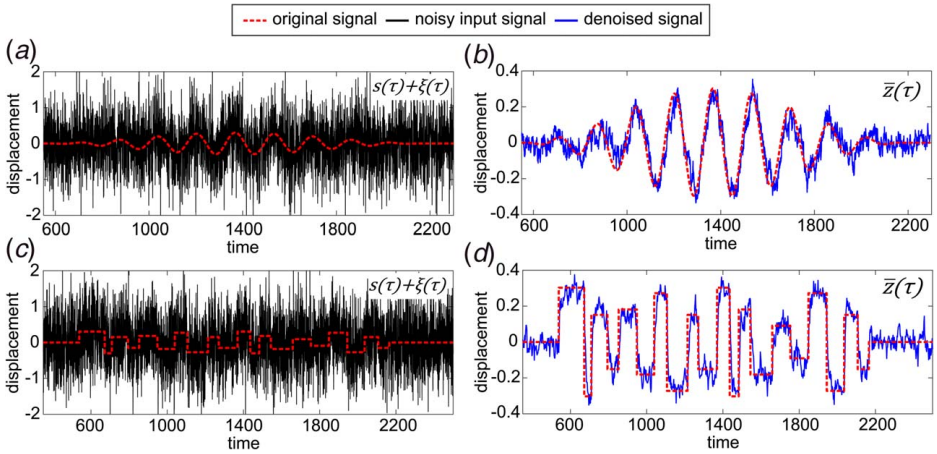

Fig. 6 (*a*) and (*c*) The original signals contaminated by noise, $D_\xi = 0.21$. (*b*) and (*d*) Denoised signals using the proposed algorithm (scaled with respect to the original signal amplitude for visual comparison). The original signals are shown (in dashed curves) in all graphs as a reference.

particular original signal waveforms; thus, the optimal noise level that provides maximum signal denoising performance could be utilized for various systems that exploit SR in array of bistable elements, as will be exemplified in Sec. 4; (3) the additional noise level D_η and gain value are adaptively determined to realize the analytically predicted optimal noise intensity D_{opt} solely based on the original attendant noise intensity D_ξ, which may be one of the few quantities that can be readily assessed from signals contaminated by severe noise; and (4) the proposed approach could be applied regardless of the waveform and amplitude of the input signal since it is based on suprathreshold SR in an array of bistable systems, provided the bistable system is designed such that the waveform varies on a time scale that is much slower than the characteristic time of the bistable system. Overall, the proposed approach yields great potential for online signal denoising in practice by requiring little information on the original input signal a priori and adaptively adjusting the additional noise level and gain values only based on the attendant noise level.

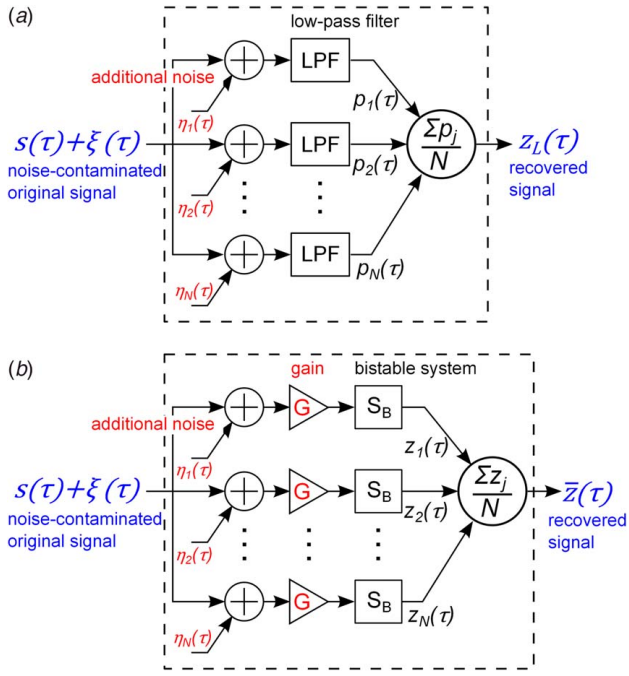

Fig. 7 Block diagrams of (*a*) LPF-based approach and (*b*) proposed SR-based method

3.2 Numerical Investigations. Numerical case studies are conducted in this section to investigate and demonstrate the effectiveness of the proposed SR-based signal denoising approach. The case study is performed by numerically integrating the nondimensional governing equation (1) to recover the original signal that is an amplitude modulated sine wave of Eq. (2). Figure 6(*a*) shows an example of a noisy signal where the original signal with peak amplitude $A = 0.3$ is contaminated by ambient noise ($D_\xi = 0.21$). The additional noise, of which intensity $D_\eta = 1.88$ is determined based on the ambient noise level, is applied to the bistable system along with the noisy input signal following gain adjustment ($G = 0.58$) to utilize the favorable operational noise level $D_{\text{opt}} = 0.72$. By averaging the output voltages of an array of 100 bistable systems, the denoised signal can be obtained as shown in Fig. 6(*b*). It can be clearly observed that the proposed SR-based approach markedly enhances the noisy signal to recover the original waveform by increasing CC from 0.16 to 0.85. The procedure is repeated for an aperiodic square wave with random amplitudes (peak amplitude $A = 0.3$) having center frequency of 0.0061 and −3 dB fractional bandwidth of 18%, where the input waveform varies on a time scale that is much slower than the characteristic time of the bistable system. The aperiodic square wave contaminated by noise ($D_\xi = 0.21$) is shown in Fig. 6(*c*). Figure 6(*d*) presents the denoised output signal where CC increased from 0.25 to 0.87. These results verify that the proposed SR-based approach effectively recovers aperiodic waveforms as well from noisy input signals.

For a comprehensive evaluation, the proposed signal denoising approach is conducted for a broad range of original signal amplitudes and attendant noise levels using the amplitude modulated sine wave in Eq. (2). In addition, the signal denoising results utilizing conventional filtering are compared with the results of the proposed SR-based approach. The average of 100 runs of low-pass filtered (LPF) noisy input signal $s(\tau) + \xi(\tau)$ with independent additive noises $\eta(\tau)$ is utilized to recover the original signal, as shown in Fig. 7(*a*). The LPF-based method was numerically conducted using the MATLAB command *lowpass* with a cutoff frequency f_c at 10 times of the excitation frequency f_o and a transition band steepness of 0.99.

The CCs between the original $s(\tau)$ and noisy input $s(\tau) + \xi(\tau)$ signals are shown in Fig. 8(*a*) as a function of the ambient noise level and original signal amplitude. The increase of darkness in the contour represents a greater CC value. It is observed from Figs. 8(*b*) and 8(*c*) that the CC values are greatly increased

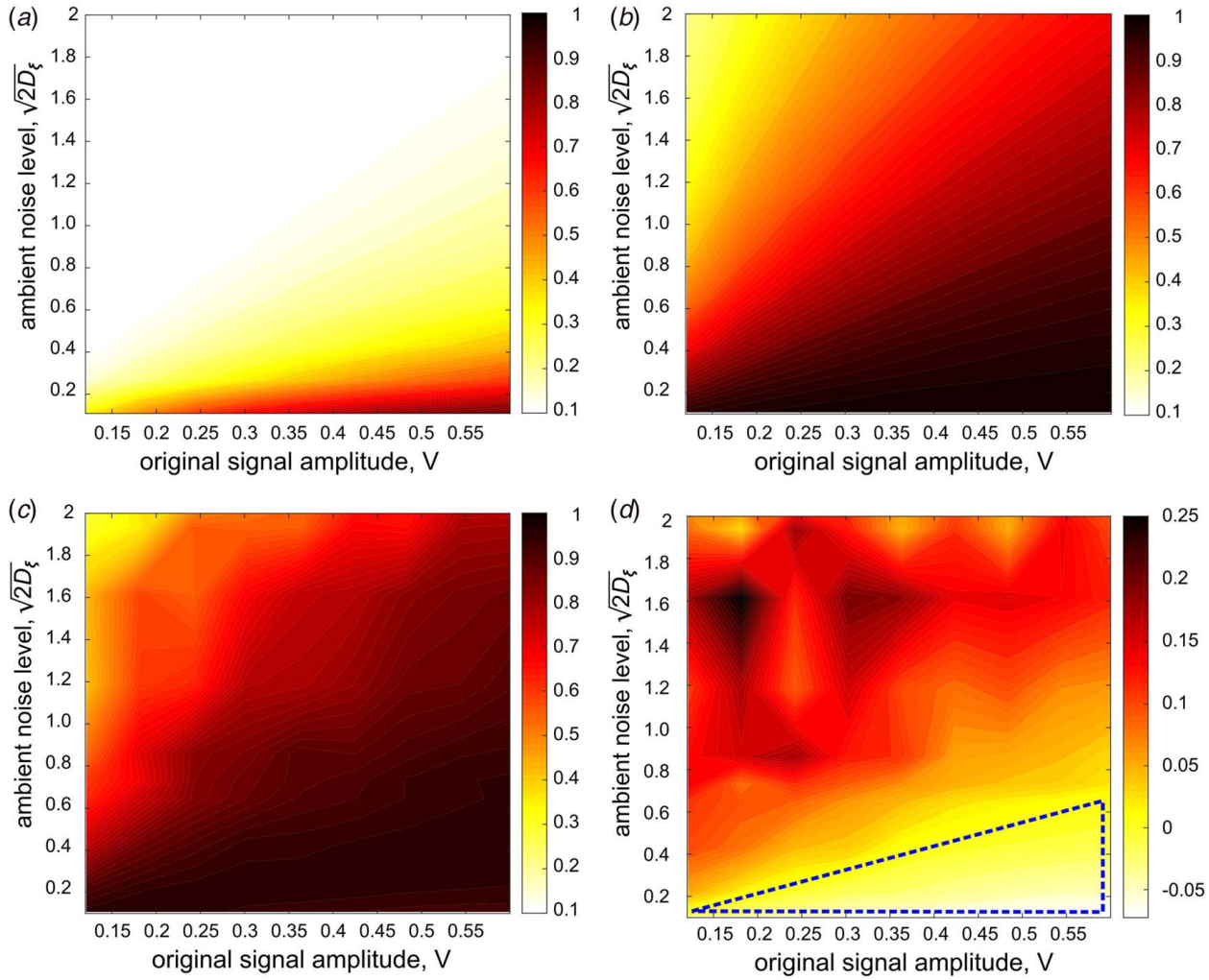

Fig. 8 CC values between the original $s(\tau)$ and noisy input $s(\tau)+\xi(\tau)$ signals for various original signal amplitudes and noise levels. Denoising performances of (*b*) the LPF-based approach and (c) the proposed SR-based method, displayed by CC between the original and denoised signals. (*d*) The difference between the CC of SR-based and LPF-based methods ($CC_{SR} - CC_{LPF}$).

compared to those of Fig. 8(*a*) when the LPF-based and the proposed SR-based denoising algorithms are respectively applied. Figure 8(*d*) displays the difference in CC values between the SR-based and LPF-based results ($CC_{SR} - CC_{LPF}$). When the original signal amplitude reduces or the attendant noise level increases, in other words, when the noise contamination is sufficiently significant, the proposed SR-based approach outperforms the LPF-based method as observed from Fig. 8(*d*) and example noisy input and recovered signals shown in Fig. 9. On the other hand, the LPF-based approach may provide greater CC values than the proposed approach when the input amplitude is relatively large with low attendant noise, as observed from the conditions highlighted by dashed lines in Figs. 8(*d*), 9(*a*), and 9(*b*). However, both methods provide CC values that are close to one for such conditions, indicating that both methods provide excellent signal denoising performance when the original signal is relatively mildly contaminated by ambient noise. Overall, the numerical investigation results validate the remarkable performance of the proposed SR-based signal denoising approach especially when the original signal is significantly contaminated by attendant noise.

4 Experimental Investigations

In this section, experimental case study results are presented to demonstrate and validate the effectiveness of the proposed SR-based signal denoising. The proposed approach is applied to recover noise-contaminated AE signals. AE is a phenomenon of transient elastic waves generated in solids when the material undergoes sudden redistribution of localized internal energy as a result of, for example, aging, temperature, pressure changes, or external mechanical loading [2,36]. Since AE signal is a high-frequency stress wave that does not require external excitation source other than the energy source from the defect occurrence, it has been widely utilized for SHM entertaining high sensitivity to small-sized damage and simple implementation [46–51]. On the other hand, since AE signals by small-sized damage may easily be buried in noise in practical implementations, signal denoising is critical for AE-based SHM [2,36,52].

The experimental proof-of-concept configuration is shown in Fig. 10(*a*). AE signals are generated by the Hsu–Nielson source method [53] at a location 50 mm away from a piezoelectric (PZT) transducer (PSI-5A4E) that is attached on the surface of an aluminum (Al-2024) beam structure. This method utilizes pencil lead break of a mechanical pencil, which generates a stress pulse (AE) due to a sudden release of mechanical stress on the target surface. Since the AE signals experimentally measured in the laboratory exhibited negligible level of noise, Gaussian white noise is added to the AE signal to generate a noise-contaminated signal following a pre-amplification of 20 dB. We employ a double-well Duffing analog circuit [54] shown in Fig. 10(*b*) as the bistable element to

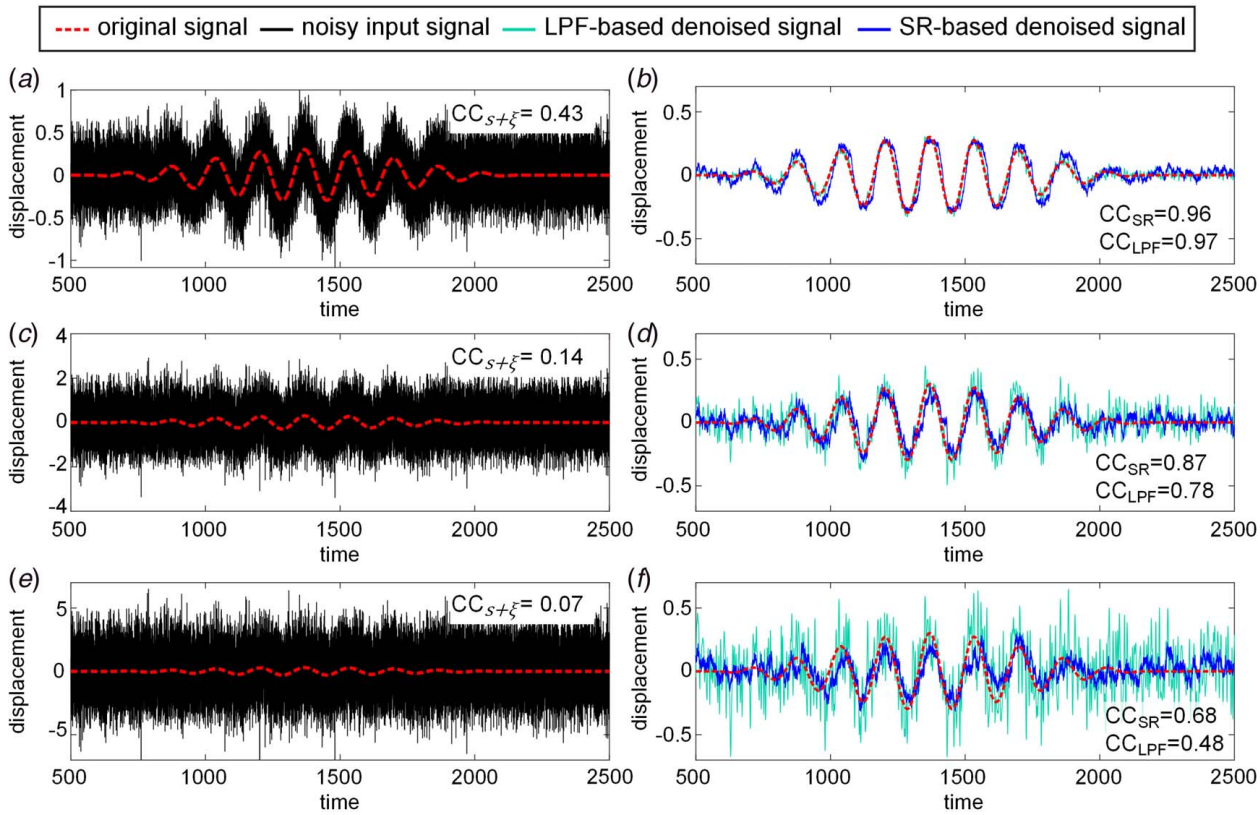

Fig. 9 Denoising results of a signal with $A = 0.3$ for three noise levels: $D_\xi = 0.02$ in row (*a*) and (*b*), $D_\xi = 0.26$ in (c) and (*d*), and $D_\xi = 1.30$ in (e) and (*f*). Noisy original signals $s(\tau) + \xi(\tau)$ are shown on the left column and the denoised signals are displayed along the right column. The original signals are included (as dashed lines) in all plots for visual comparison. The CC values are given next to each result in all plots.

realize SR. This circuit exhibits bistability with piecewise-linear characteristics introduced by the nonlinear feedback loop among the op-amp and diodes. The bistable circuit involves saddle-node bifurcation that activates sudden transitions between the intrawell and interwell oscillations. As a result, bistable circuits have been applied for various bifurcation-based applications [37,39,55–59]. Since this bistable circuit design exhibits negligible backward coupling due to the characteristics of op-amp, it is suitable to utilize as a signal conditioning device that has little effect on the input signal [37]. Considering that the frequency range of AE signals is generally known to be approximately between 150 and 300 kHz [36], the bistable circuit is designed to exhibit linear resonance frequency at 13 MHz, approximately 50 times higher than the frequency range of AE signals. The op-amp is TLE2141CP and the diodes are 1N4148. Table 1 provides relevant parameters of the beam structure, piezoelectric transducer, and bistable circuit used in the experimental study. In this experimental investigation, we have employed a proof-of-concept platform that exploits an iterative method with a bistable circuit to realize the proposed denoising algorithm. Instead of utilizing the noise-contaminated AE signal as an input simultaneously fed to an array of 100 bistable circuits, the noisy AE signal is first recorded using the data acquisition system (NI

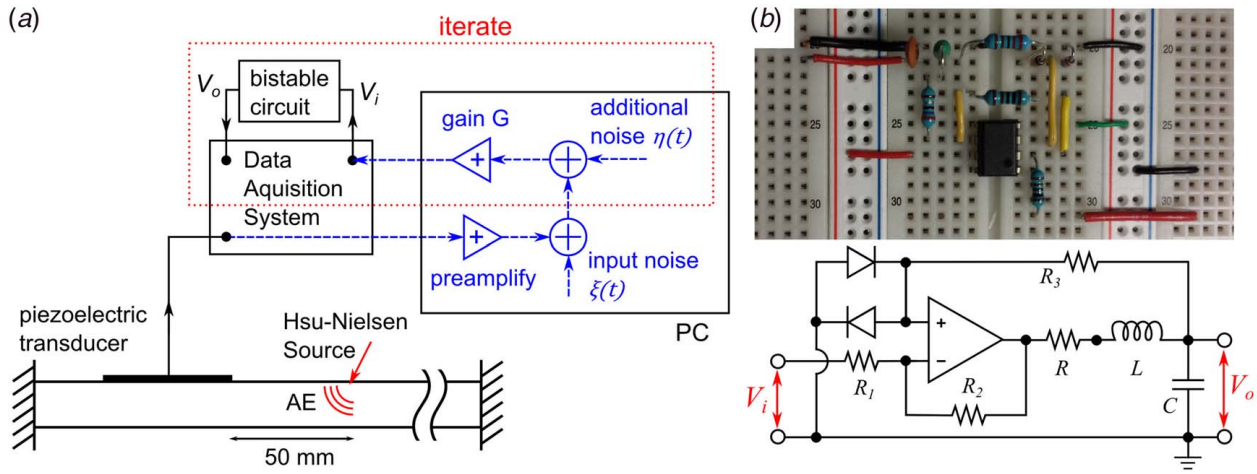

Fig. 10 (*a*) Schematic diagram of the experimental proof-of-concept configuration. The dashed lines indicate data processed in a PC and (*b*) Bistable circuit and its diagram utilized in the experiment.

Table 1 Experimental system parameters

Beam (mm)	627.2 × 7.21 × 3.175		PZT (mm)	16.85 × 7.09 × 0.191	
L (uH)	C (pF)	R (Ω)	R_1 (kΩ)	R_2 (kΩ)	R_3 (kΩ)
0.22	680	27	1	1	2

PXIe-6124) and the attendant noise level is assessed. Then the recorded signal is iteratively fed to a bistable circuit for 100 runs. For each iteration, independent additive noise is applied to the noisy AE signal following gain adjustment. The responses of the bistable circuit are then recorded for each iteration and averaged to recover the original signal once all the iterations are completed. The time delay induced by the analog-to-digital and digital-to-analog conversion processes in the experimental investigations was numerically compensated. The gain G is determined so that the total noise (summation of original attendant noise and additional noise) intensity matches the optimal value. Since the optimal noise intensity ($D_{\text{opt}} = 0.72$) determined in Sec. 2 is the optimal value for a non-dimensional bistable Duffing system, we approximated the bistable circuit as a double-well Duffing oscillator [56] and obtained the optimal noise intensity ($\bar{D}_{\text{opt}} = 0.5\ V^2$) for the bistable circuit by a series of back calculations. A more detailed discussion is given in Appendix B.

Figure 11 illustrates denoising results of an AE signal with three different ambient noise levels ($\sqrt{2D_\xi}$) of 100, 150, and 200 mV root-mean-square (RMS) in row (a, b), (c, d), and (e, f), respectively. It can be clearly observed that the noisy AE signals shown on the left column of Fig. 11 are effectively denoised for all three noise levels by employing the proposed algorithm and recovered as shown on the right column. Figure 12 presents a quantitative evaluation of the denoising performance for the three different noise levels by comparing the values of CC before and after the denoising algorithm is applied. The bar heights indicate mean values of the CC determined from 10 AE experiments, while the error bars show one standard deviation from the mean. The mean values of CC increase for all three noise levels, which reflects that the recovered waveform fidelity is improved when the proposed denoising algorithm is applied. Since the proof-of-concept iterative approach was based on utilizing the data acquisition system that is capable of both generating and measuring analog signals, the cutoff frequency of the white noise generated in the experimental investigations was limited to $F_s = 4$ MHz by the maximum sampling rate for the analog output of the equipment. This cutoff frequency yields F_s/f_o ratio approximately 17.7 based on the peak frequency ($f_o \approx$ 227 kHz) of the experimental AE signal identified from its power spectrum. On the other hand, as illustrated in the numerical investigation results provided in Appendix C, it is envisioned that the experimental signal denoising performance would be greatly improved when white noise that has significantly higher cutoff frequency than the frequency band of the original AE signal is employed, because the SR is based on the assumption that the original input signal varies much slower than the stochastic influences [60,61].

Overall, the experimental investigation results validate the effectiveness of the proposed SR-based signal denoising method. In addition, it is worth noting that the proposed denoising approach adaptively determines the optimal additional noise level and gain

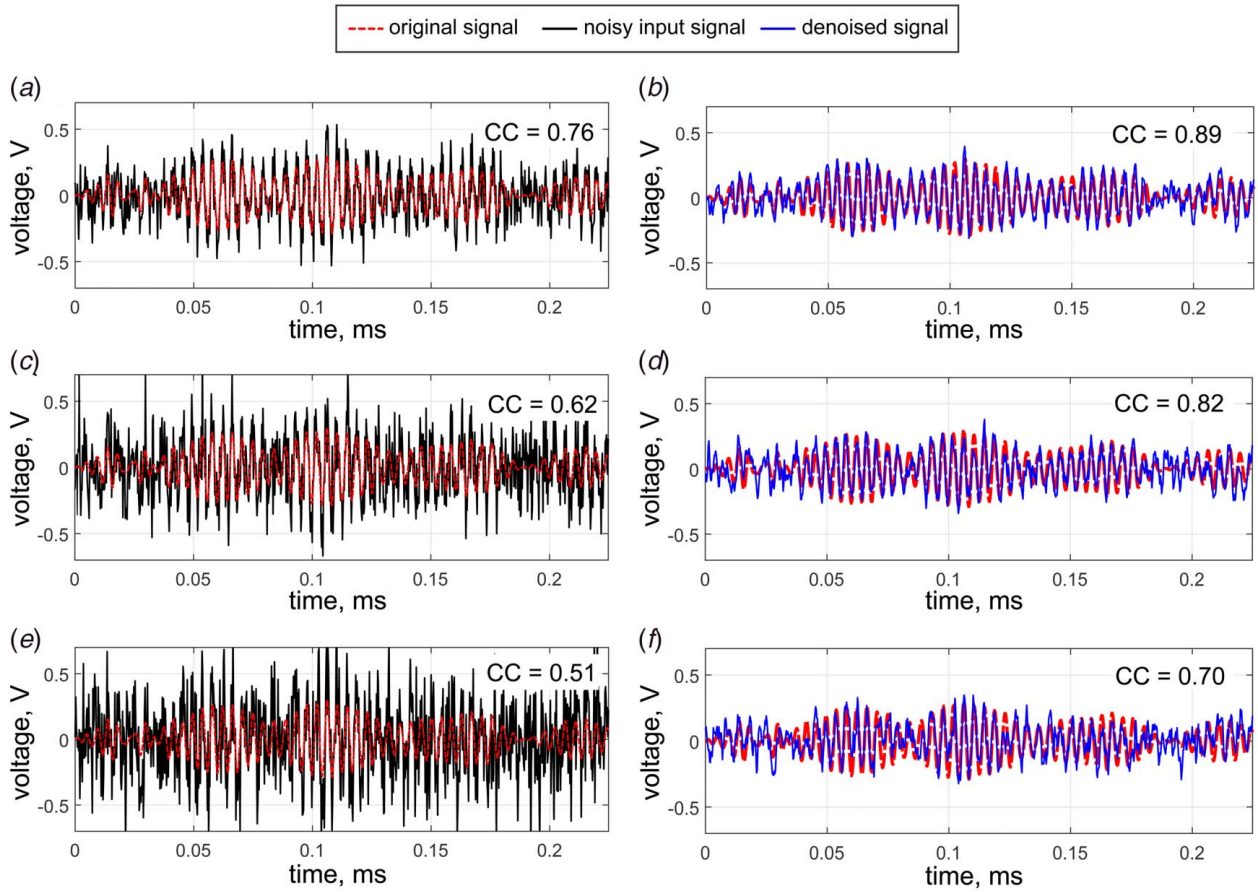

Fig. 11 Experimental denoising results of AE signals contaminated by three noise levels: row (a) and (b) = 100 mV RMS, (c) and (d) = 150 mV RMS, and (e) and (f) = 200 mV RMS. Noisy AE signals are shown on the left column and the denoised signals (normalized with respect to the original signal amplitude) are displayed along the right column. The original AE signals are included (in dashed lines) in all plots for visual comparison. The CC values are given next to each result in all plots.

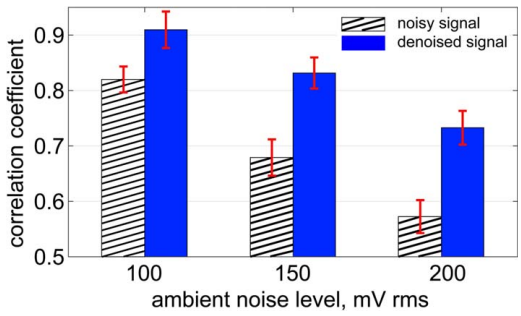

Fig. 12 Denoising performance (CC) for different ambient noise levels. Error bars indicate one standard deviation from the mean.

values based on the analytically estimated optimal noise level and the readily assessable ambient noise intensity without employing any sophisticated algorithms that often require a post-processing environment, thus suitable for online signal denoising.

5 Summary and Conclusion

This research investigates a novel online signal denoising approach that exploits adaptive SR phenomena in a parallel array of bistable systems. The proposed approach adaptively applies additional noise to the noise-contaminated input signal following gain adjustments to utilize the analytically estimated optimal noise level providing reliable signal denoising performance for a wide range of original signal amplitudes. The original signal is recovered by averaging out the noise-induced stochastic transitions in the responses of the array of bistable systems. The proposed method does not require operating computationally expensive optimization algorithms in a post-processing environment for selecting scaling parameters, thus enabling online signal denoising. The additional noise level and gain values are determined solely based on the ambient noise level which may be one of the few quantities that can be easily assessed from severely noise-contaminated signals in practice. The optimal noise intensity theoretically estimated in this study is determined based on a generalized bistable Duffing oscillator without any reference to particular original signal waveforms. Therefore, the optimal noise level could be practically utilized for various systems that exploit SR in an array of bistable elements. Numerical investigation results reveal the effectiveness of the denoising strategy for both periodic and aperiodic signals that are often observed in practice. Compared to conventional low-pass filtering, the proposed SR-based approach outperforms the LPF-based method when the ambient noise is sufficiently large. On the other hand, when the original signal is relatively mildly contaminated by ambient noise, the LPF-based approach may provide higher CC values than the proposed approach, while both SR-based and LPF-based methods provide excellent signal denoising performance. Experimental validation with denoising AE signals by employing a proof-of-concept bistable analog circuit system demonstrates that the new approach substantially enhances the signal quality by only utilizing the ambient noise intensity to adaptively determine the gain and additional noise level without any sophisticated post-processing. Overall, the results of this study show promising potential of the new denoising strategy as an effective online preprocessor for a broad range of applications where little information is known a priori about the original signal.

Acknowledgment

This research is partially supported by the University of Michigan Collegiate Professorship. J.K. acknowledges start-up funds from the Department of Mechanical Engineering at Georgia Southern University. The authors are also grateful to Professor Jerome P. Lynch and Professor Carlos E. S. Cesnik at the University of Michigan for generously providing access to data acquisition systems for the experimental investigation.

Conflict of Interest

There are no conflicts of interest.

Data Availability Statement

The datasets generated and supporting the findings of this article are obtained from the corresponding author upon reasonable request. The authors attest that all data for this study are included in the paper. Data provided by a third party are listed in Acknowledgment.

Appendix A

The input signal $s(\tau)$ contaminated by additional noise $\eta_f(\tau)$, shown in Fig. 2(*a*), was LPF with a cutoff frequency f_c at the excitation frequency f_o using the MATLAB command *lowpass*. Compared to the LPF result shown in Fig. 13(*a*), the proposed SR-based method yields a superior signal denoising performance as presented in Fig. 13(*b*). In addition, the denoising performance (CC) of low-pass filtering is significantly dependent on selecting the cutoff frequency as illustrated in Fig. 13(*c*), which may be challenging to find the optimal cutoff frequency that often depends on the original waveform parameters, especially when the signal of interest

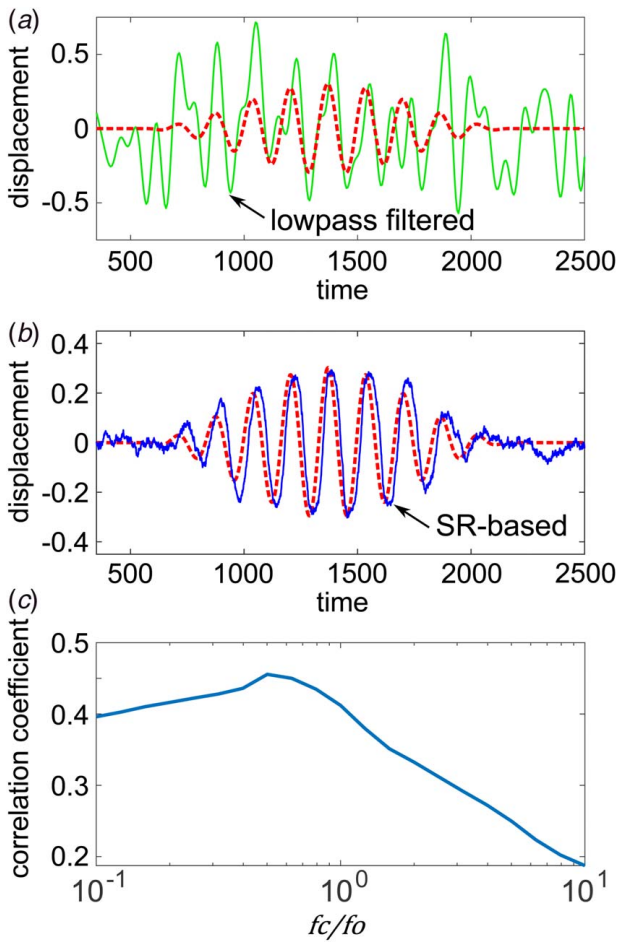

Fig. 13 Denoised signals obtained by (*a*) low-pass filtering and (*b*) the proposed SR-based approach. Dashed curves in both figures indicate the original signal. (c) Denoising performance of low-pass filtering depending on the cutoff frequency.

is corrupted by noise in practice. On the other hand, the proposed SR-based approach may reliably recover the original signal since the optimal noise intensity for SR can be determined solely based on the original attendant noise intensity $D_{\bar{\xi}}$, which may be one of the few quantities that can be readily assessed from signals contaminated by severe noise. Furthermore, the proposed approach could be applied regardless of the exact waveform and amplitude of the input signal, provided that the bistable system is designed such that its linear natural frequency is much greater than the frequency band of the original signal.

Appendix B

Assuming the qualitative piecewise-linear characteristics of the nonlinear restoring function $F(V_o)$ of the double-well Duffing analog circuit as a cubic polynomial $-\alpha V_o + \beta V_o^3$, the governing equation can be approximated as a conventional double-well Duffing equation that has a restoring force expressed by a cubic polynomial with negative linear and positive cubic terms [56]:

$$\mathrm{LC}\ddot{V}_o(t) + \mathrm{RC}\dot{V}_o(t) - \alpha V_o(t) + \beta V_o(t)^3 = \bar{A}\sin\bar{\omega}t + \bar{\nu}(t) \qquad \text{(B1)}$$

where L, C, and R represent the circuit inductance, capacitance, and resistance, respectively; $\bar{A}\sin\bar{\omega}t$ and $V_o(t)$, respectively, indicate the input and output voltages of the circuit with amplitude $\bar{A}$ and frequency $\bar{\omega}$; $\bar{\nu}(t)$ is zero-mean Gaussian white noise with autocorrelation $\bar{\nu}(t)\bar{\nu}(0) = 2\bar{D}_\nu\delta(t)$; the overdot indicates the time derivative. Figure 14 shows that the polynomial fit ($\alpha = 0.643$ and $\beta = 0.389$) effectively emulates the global characteristics of the experimentally obtained nonlinear voltage function, yielding a high value of R^2 fitness (90.0%).

Considering a heavily damped motion of a particle in a symmetric double-well potential, we approximate Eq. (B1) as a periodically modulated Langevin equation by ignoring the inertia of the particle [16]

$$\tau_o\dot{V}_o(t) = \frac{1}{\mathrm{LC}}(\alpha V_o - \beta V_o^3 + A\sin\omega\tau + \nu(\tau)) \qquad \text{(B2)}$$

where $\tau_o = R/L$ is a time constant related to the damping of the system. By introducing a non-dimensional parameter $z = V_o/\sqrt{\alpha/\beta}$ and time $\tau = \alpha(t/\mathrm{RC})$, a dimensionless equation is obtained as

$$z'(\tau) = z(\tau) - z^3(\tau) + A\sin\omega\tau + \nu(\tau) \qquad \text{(B3)}$$

where the operator $(\,)'$ represents differentiation with respect to non-dimensional time τ and autocorrelation $\nu(\tau)\ \nu(0) = 2D\delta(\tau)$. The following parameters are defined:

$$\omega = \frac{RC}{\alpha}\bar{\omega};\ A = \frac{\bar{A}}{\alpha\sqrt{\alpha/\beta}};\ D = \bar{D}_\nu\frac{\beta}{\alpha^3} \qquad \text{(B4)}$$

By straightforward back calculations, the optimal noise $D_{\mathrm{opt}} \approx 0.72$ obtained from Sec. 3.1 can be used to determine

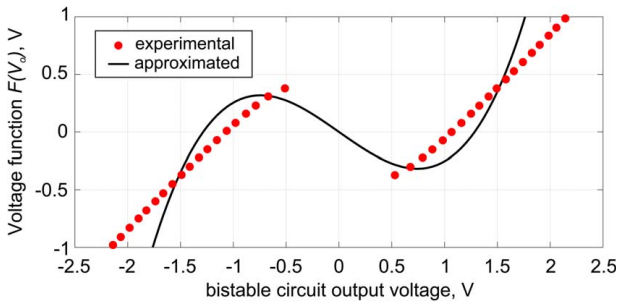

Fig. 14 Experimentally measured (circles) nonlinear voltage function with respect to output voltage amplitude. The cubic polynomial fit (solid curve) yields R^2 fitness of 0.9.

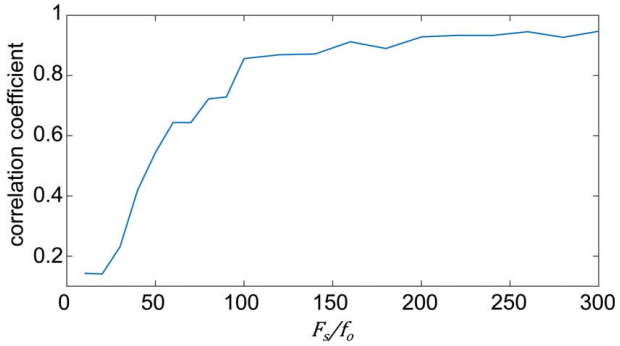

Fig. 15 Denoising performance (CC) as a function of *Fsfo* ratio

$\bar{D}_{\mathrm{opt}} \approx 0.5\ V^2$, the optimal intensity of total noise applied to the bistable circuit. The gain G is then determined by Eq. (10) based on the ambient noise level.

Appendix C

The numerical case study shown in Fig. 2 is repeated for different noise bandwidths to investigate the influence of noise bandwidth on the signal denoising performance. Figure 15 illustrates that the signal denoising performance (CC) is significantly deteriorated when the ratio between the white noise bandwidth F_s and the original signal frequency f_o becomes smaller, because the SR is based on the assumption that the original input signal varies much slower than the stochastic influences [60,61]. Thus, as shown in Fig. 15, the experimental signal denoising performance presented in Sec. 4 would be greatly improved by employing white noise that has considerably higher cutoff frequency than the frequency band of the original AE signal.

References

[1] Farrar, C., and Worden, K., 2007, "An Introduction to Structural Health Monitoring," Philos. Trans. R. Soc. Lond. A, **365**(1851), pp. 303–315.
[2] Grosse, C., and Ohtsu, M., eds., 2008, *Acoustic Emission Testing*, Springer-Verlag, Berlin.
[3] Qin, Z., Chen, L., and Bao, X., 2012, "Wavelet Denoising Method for Improving Detection Performance of Distributed Vibration Sensor," IEEE Photon. Technol. Lett., **24**(7), pp. 542–544.
[4] Lei, Y., He, Z., Zi, Y., and Hu, Q., 2007, "Fault Diagnosis of Rotating Machinery Based on Multiple ANFIS Combination With GAs," Mech. Syst. Signal Process., **21**(55), pp. 2280–2294.
[5] Benzi, R., Sutera, A., and Vulpiani, A., 1981, "The Mechanism of Stochastic Resonance," J. Phys. A: Math. Gen., **14**(11), pp. L453–L457 .
[6] Nicolis, C., and Nicolis, G., 1981, "Stochastic Aspects of Climatic Transitions—Additive Fluctuations," Tellus, **33**(3), pp. 225–234.
[7] McNamara, B., Wiesenfeld, K., and Roy, R., 1988, "Observation of Stochastic Resonance in a Ring Laser," Phys. Rev. Lett., **60**(25), pp. 2626–2629.
[8] Badzey, R., and Mohanty, P., 2005, "Coherent Signal Amplification in Bistable Nanomechanical Oscillators by Stochastic Resonance," Nature, **437**(7061), pp. 995–998.
[9] Leonard, D., and Reichl, L., 1994, "Stochastic Resonance in a Chemical-Reaction," Phys. Rev. E, **49**(2), pp. 1734–1737.
[10] Yang, L., Hou, Z., and Xin, H., 1999, "Stochastic Resonance in the Absence and Presence of External Signals for a Chemical Reaction," J. Chem. Phys., **110**(7), pp. 3591–3595.
[11] Douglass, J., Wilkens, L., Pantazelou, E., and Moss, F., 1993, "Noise Enhancement of Information Transfer in Crayfish Mechanoreceptors by Stochastic Resonance," Nature, **365**(6444), pp. 337–340.
[12] Hänggi, P., 2002, "Stochastic Resonance in Biology How Noise Can Enhance Detection of Weak Signals and Help Improve Biological Information Processing," ChemPhysChem, **3**(3), pp. 285–290.
[13] Valenti, D., Fiasconaro, A., and Spagnolo, B., 2004, "Stochastic Resonance and Noise Delayed Extinction in a Model of Two Competing Species," Physica A, **331**(3), pp. 477–486.
[14] Kuperman, M., and Zanette, D., 2002, "Stochastic Resonance in a Model of Opinion Formation on Small-World Networks," **26**(3), pp. 387–391 .
[15] Meyer, B., 2017, "Optimal Information Transfer and Stochastic Resonance in Collective Decision Making," Swarm Intell., **11**(2), pp. 131–154.
[16] Gammaitoni, L., Hänggi, P., Jung, P., and Marchesoni, F., 1998, "Stochastic Resonance," Rev. Mod. Phys., **70**(1), pp. 223–287.

[17] McNamara, B., and Wiesenfeld, K., 1989, "Theory of Stochastic Resonance," Phys. Rev. A, **39**(9), pp. 4854–4869.
[18] Collins, J., Chow, C., and Imhoff, T., 1995, "Stochastic Resonance Without Tuning," Nature, **376**(6537), pp. 236–238.
[19] Mori, T., and Kai, S., 2002, "Noise-Induced Entrainment and Stochastic Resonance in Human Brain Waves," Phys. Rev. Lett., **88**(21), p. 218101.
[20] Rallabandi, V., and Roy, P., 2010, "Magnetic Resonance Image Enhancement Using Stochastic Resonance in Fourier Domain," Magn. Reson. Imag., **28**(9), pp. 1361–1373.
[21] Feng, X., Liu, H., Huang, N., Wang, Z., and Zhang, Y., 2019, "Reconstruction of Noisy Images Via Stochastic Resonance in Nematic Liquid Crystals," Sci. Rep., **9**(1), pp. 1–9 .
[22] Qiao, Z., Lei, Y., and Li, N., 2019, "Applications of Stochastic Resonance to Machinery Fault Detection: A Review and Tutorial," Mech. Syst. Signal Process., **122**, pp. 502–536.
[23] Qin, Y., Tao, Y., He, Y., and Tang, B., 2014, "Adaptive Bistable Stochastic Resonance and Its Application in Mechanical Fault Feature Extraction," J. Sound Vib., **333**(26), pp. 7386–7400.
[24] Qiao, Z., Lei, Y., Lin, J., and Jia, F., 2017, "An Adaptive Unsaturated Bistable Stochastic Resonance Method and Its Application in Mechanical Fault Diagnosis," Mech. Syst. Signal Process., **84**, pp. 731–746.
[25] Lai, Z., and Leng, Y., 2016, "Weak-Signal Detection Based on the Stochastic Resonance of Bistable Duffing Oscillator and Its Application in Incipient Fault Diagnosis," Mech. Syst. Signal Process., **81**, pp. 60–74.
[26] Lu, S., Zheng, P., Liu, Y., Cao, Z., Yang, H., and Wang, Q., 2019, "Sound-Aided Vibration Weak Signal Enhancement for Bearing Fault Detection by Using Adaptive Stochastic Resonance," J. Sound Vib., **449**, pp. 18–29.
[27] Li, J., Zhang, J., Li, M., and Zhang, Y., 2019, "A Novel Adaptive Stochastic Resonance Method Based on Coupled Bistable Systems and Its Application in Rolling Bearing Fault Diagnosis," Mech. Syst. Signal Process., **114**, pp. 128–145.
[28] He, B., Huang, Y., Wang, D., Yan, B., and Dong, D., 2019, "A Parameter-Adaptive Stochastic Resonance Based on Whale Optimization Algorithm for Weak Signal Detection for Rotating Machinery," Measurement, **136**, pp. 658–667.
[29] Wang, S., Niu, P., Guo, Y., Wang, F., Li, W., Shi, H., and Han, S., 2020, "Early Diagnosis of Bearing Faults Using Decomposition and Reconstruction Stochastic Resonance System," Measurement, **158**, p. 107709.
[30] Fu, Y., Kang, Y., and Liu, R., 2020, "Novel Bearing Fault Diagnosis Algorithm Based on the Method of Moments for Stochastic Resonant Systems," IEEE Trans. Instrum. Meas., **70**, pp. 1–10 .
[31] Dong, H., Wang, H., Shen, X., and Jiang, Z., 2018, "Effects of Second-Order Matched Stochastic Resonance for Weak Signal Detection," IEEE Access, **6**, pp. 46505–46515.
[32] Xu, B., Duan, F., Bao, R., and Li, J., 2002, "Stochastic Resonance With Tuning System Parameters: The Application of Bistable Systems in Signal Processing," Chaos Solitons Fractals, **13**(4), pp. 633–644.
[33] Xu, B., Li, J., and Zheng, J., 2003, "How to Tune the System Parameters to Realize Stochastic Resonance," J. Phys. A: Math. Gen., **36**(48), pp. 11969–11980.
[34] Collins, J., Chow, C., Capela, A., and Imhoff, T., 1996, "Aperiodic Stochastic Resonance," Phys. Rev. E, **54**(5), pp. 5575–5584.
[35] Stocks, N., 2000, "Suprathreshold Stochastic Resonance in Multilevel Threshold Systems," Phys. Rev. Lett., **84**(11), pp. 2310–2313.
[36] Hellier, C., 2001, *Handbook of Nondestructive Evaluation*, McGraw-Hill Professional, New York.
[37] Harne, R. L., and Wang, K. W., 2013, "Robust Sensing Methodology for Detecting Change With Bistable Circuitry Dynamics Tailoring," Appl. Phys. Lett., **102**(20), p. 203506.
[38] Szemplińska-Stupnicka, W., and Rudowski, J., 1993, "Steady States in the Twin-Well Potential Oscillator: Computer Simulations and Approximate Analytical Studies," Chaos, **3**(3), pp. 375–385.
[39] Kim, J., and Wang, K. W., 2018, "Predicting Non-stationary and Stochastic Activation of Saddle-Node Bifurcation in Non-smooth Dynamical Systems," Nonlinear Dyn., **93**(2), pp. 251–258.
[40] Hansen, J., and Penland, C., 2006, "Efficient Approximate Techniques for Integrating Stochastic Differential Equations," Mon. Weather Rev., **134**(10), pp. 3006–3014.
[41] Mukaka, M., 2012, "A Guide to Appropriate Use of Correlation Coefficient in Medical Research," Malawi Med. J., **24**(3), pp. 69–71.
[42] Dykman, M., Mannella, R., McClintock, P., and Stocks, N., 1992, "Phase Shifts in Stochastic Resonance," Phys. Rev. Lett., **68**(20), pp. 2985–2988.
[43] Chapeau-Blondeau, F., and Godivier, X., 1997, "Theory of Stochastic Resonance in Signal Transmission by Static Nonlinear Systems," Phys. Rev. E, **55**(2), pp. 1478–1495.
[44] Duan, F., Chapeau-Blondeau, F., and Abbott, D., 2008, "Stochastic Resonance in a Parallel Array of Nonlinear Dynamical Elements," Phys. Lett. A, **372**(13), pp. 2159–2166.
[45] McDonnell, M., and Abbott, D., 2009, "What Is Stochastic Resonance? Definitions, Misconceptions, Debates, and Its Relevance to Biology," PLoS Comput. Biol., **5**(5), p. e1000348.
[46] Behnia, A., Chai, H., and Shiotani, T., 2014, "Advanced Structural Health Monitoring of Concrete Structures With the Aid of Acoustic Emission," Constr. Build. Mater., **65**, pp. 282–302.
[47] Nair, A., and Cai, C., 2010, "Acoustic Emission Monitoring of Bridges: Review and Case Studies," Eng. Struct., **32**(6), pp. 1704–1714.
[48] Eaton, M., Pullin, R., and Holford, K., 2012, "Towards Improved Damage Location Using Acoustic Emission," Proc. Inst. Mech. Eng. C J. Mech. Eng. Sci., **226**(9), pp. 2141–2153.
[49] Inasaki, I., 1998, "Application of Acoustic Emission Sensor for Monitoring Machining Processes," Ultrasonics, **26**(1–5), pp. 273–281.
[50] Li, X., 2002, "A Brief Review: Acoustic Emission Method for Tool Wear Monitoring During Turning," Int. J. Mach. Tools Manuf., **42**(2), pp. 157–165.
[51] Lédeczi, Á., Hay, T., Volgyesi, P., Hay, D., Nádas, A., and Jayaraman, S., 2009, "Wireless Acoustic Emission Sensor Network for Structural Monitoring," IEEE Sens. J., **9**(11), pp. 1370–1377.
[52] Tan, A., Kaphle, M., and Thambiratnam, D., 2009, "Structural Health Monitoring of Bridges Using Acoustic Emission Technology," 8th International Conference on Reliability, Maintainability and Safety, 2009 (ICRMS 2009), Chengdu, China, July 20–24, pp. 839–843.
[53] A. E976-99, 2009, *Standard Guide for Determining the Reproducibility of Acoustic Emission Sensor Response*, American Society for Testing and Materials.
[54] Tamaševičius, A., Mykolaitis, G., Pyragas, V., and Pyragas, K., 2007, "Delayed Feedback Control of Periodic Orbits Without Torsion in Nonautonomous Chaotic Systems: Theory and Experiment," Phys. Rev. E, **76**(2), p. 026203.
[55] Kim, J., Harne, R. L., and Wang, K. W., 2015, "Enhancing Structural Damage Identification Robustness to Noise and Damping With Integrated Bistable and Adaptive Piezoelectric Circuitry," ASME J. Vib. Acoust., **137**(1), p. 011003.
[56] Kim, J., Harne, R. L., and Wang, K. W., 2016, "Predicting Non-stationary and Stochastic Activation of Saddle-Node Bifurcation," ASME J. Comput. Nonlinear Dyn., **12**(1), p. 011009.
[57] Kim, J., and Wang, K. W., 2019, "Electromechanical Impedance-Based Damage Identification Enhancement Using Bistable and Adaptive Piezoelectric Circuitry," Struct. Health Monit., **18**(4), pp. 1268–1281.
[58] Yang, K., Zhang, Z., Zhang, Y., and Huang, H., 2019, "High-Resolution Monitoring of Aerospace Structure Using the Bifurcation of a Bistable Nonlinear Circuit With Tunable Potential-Well Depth," Aerosp. Sci. Technol., **87**, pp. 98–109.
[59] Harne, R. L., and Wang, K. W., 2017, *Harnessing Bistable Structural Dynamics: For Vibration Control, Energy Harvesting and Sensing*, John Wiley & Sons, Hoboken, NJ.
[60] Harmer, G., Davis, B., and Abbott, D., 2002, "A Review of Stochastic Resonance: Circuits and Measurement," IEEE Trans. Instrum. Meas., **51**(2), pp. 299–309.
[61] Berglund, N., and Gentz, B., 2006, *Noise-Induced Phenomena in Slow-Fast Dynamical Systems: A Sample-Paths Approach*, Springer Science & Business Media, Berlin.